Journal of the Brazilian Society of Mechanical Sciences and Engineering (2020) 42:118
https://doi.org/10.1007/s40430-019-2151-7

TECHNICAL PAPER

Vibration analysis of cantilever FG-CNTRC trapezoidal plates

Mohammad Hossein Majidi[1] · Mohammad Azadi[1] · Hamidreza Fahham[1]

Received: 5 September 2019 / Accepted: 12 December 2019 / Published online: 7 February 2020

Abstract

In this paper, a numerical solution is presented for free vibration analysis of cantilever functionally graded carbon nanotube-reinforced trapezoidal plates. The plate is modeled based on the first-order shear deformation theory, effective mechanical properties are estimated according to extended rule of mixture, and the set of governing equations and boundary conditions are derived using Hamilton's principle. Generalized differential quadrature method is employed, and natural frequencies and corresponding mode shapes are derived numerically. Convergence and accuracy of the solution are confirmed, and effect of various parameters on the natural frequencies is investigated including geometrical characteristics, volume fraction and distribution of carbon nanotubes. Because of similarity of the studied model with the wing, tail and fin of aircrafts and missiles, results of this paper can be useful in design and analysis of aeronautic vehicles in the near future. It is worth mentioning that results of this paper may serve as benchmarks for future studies.

Keywords Vibration · Carbon nanotubes · Trapezoidal plate · First-order shear deformation theory

1 Introduction

Due to their superior mechanical, thermal and electrical properties, CNTs can be utilized in many applications including the reinforcement of polymer composites, such as CNTRC beams, plates and shells. So, since the discovery of CNTs by Ijima [1] in 1991, many researchers have investigated their unique capabilities as reinforcements in composite structures. On the other hand, trapezoidal plates are widely used in mechanical, civil and aeronautical engineering applications such as bridges, wings, tails and fins of aircrafts. However, due to the mathematical difficulties and complexities involved in formulation, mechanical analysis of CNTRC trapezoidal plates is poorly investigated in comparison with those of rectangular, skew and circular plates [2–7].

In recent years, some authors focused on the bending, buckling and vibration analyses of CNTRC rectangular and skew plates. Based on FSDT, Zhu et al. [8] presented an element for bending and free vibration analyses of CNTRC moderately thick rectangular plates. They investigated influences of distribution and volume fractions of CNTs, boundary conditions and edge-to-thickness ratio on the bending characteristics, natural frequencies and mode shapes of the plate. Zhang et al. [9, 10] used FSDT and element-free IMLS-Ritz method and focused on the free flexural vibration analysis of FG-CNTR triangular and skew plates. They presented new sets of natural frequencies and mode shapes for various FG-CNTRC triangular and skew plates and studied effect of volume fraction and distribution of CNTs, plate thickness-to-width ratio, plate aspect ratio and boundary condition on the natural frequencies of plates. In a similar work, Zhang et al. [11] studied free vibration analysis of triangular plates subjected to in-plane stresses. In this case, they studied effect of in-plane stress on the natural frequencies of the plate. Again with similar theory for modeling of plate and method of solution, Lei et al. [12] focused on free flexural vibration analysis of FG-CNTRC quadrilateral plates resting on Pasternak foundations. For different boundary conditions, they presented a parametric study on natural frequencies for various types of CNTs distributions, volume fraction of CNTs and geometries parameters of the plate.

Based on FSDT, García-Macías et al. [13] presented an element for static and dynamic simulations of moderately thick FG-CNTRC skew plates with arbitrary-oriented reinforcements. They investigated a parametric study to

Technical Editor: Thiago Ritto.

Mohammad Azadi
mazadi@miau.ac.ir

[1] Depratment of Mechanical Engineering, Marvdasht Branch, Islamic Azad University, Marvdasht, Iran

investigate influences of skew angle, fiber orientation, distribution and volume fraction of CNTs, thickness-to-width ratio, aspect ratio and boundary conditions on deflection and natural frequencies of FG-CNTRC skew plates. Lei et al. [14] employed FSDT and kp-Ritz method and studied free vibration analysis of laminated FG-CNTRC rectangular plates. They focused on the effects of lamination angle, number of layers, distributions and volume fractions of CNTs, plate width-to-thickness ratio and plate aspect ratio on the natural frequencies of laminated FG-CNTRC rectangular plates with various boundary conditions. Using third-order shear deformation theory (TSDT), Mori–Tanaka method and method of calculating the average stress of composite materials, Guo and Zhang [15] studied nonlinear vibration behaviors of CNTRC rectangular plates under combined dynamic axial and transverse excitations. They investigated effects of the forcing excitations on the different kinds of the periodic and chaotic motions of the CNTRC plates through a comprehensive parametric study.

Based on a higher-order shear deformation theory (HSDT) and using element-free kp-Ritz method, Selim et al. [16] studied free vibration analysis of CNTRC rectangular plates in a thermal environment. They studied effects of volume fraction and distribution of CNTs, boundary conditions, plate aspect ratio, plate thickness-to-width ratio and CNT volume fraction on the natural frequencies and sequence of first six mode shapes. Using FSDT and element-free improved moving least-squares Ritz (IMLS-Ritz) method, Zhang et al. [17] studied free vibration analysis of FG-CNTRC moderately thick rectangular plates with edges elastically restrained against transverse displacements and rotation. Besides volume fraction and distribution of CNTs and also geometrical parameters, they focused on the effect of elastically restrained edges on the natural frequencies of the plate. Zhang and Selim [18] employed an HSDT along with element-free IMLS-Ritz method and focused on free vibration behavior of FG-CNTRC thick laminated composite plates. For various CNT orientation angles and boundary conditions, they presented a parametric study to show effects of CNT volume fraction, plate aspect ratio, plate width-to-thickness ratio and number of plate's layers on natural frequencies of the plate. Employing FSDT along with Ritz method, Kiani et al. [19] focused on the free vibration analysis of FG-CNTRC skew plates. For various types of boundary conditions, he studied effect of aspect ratio, thickness-to-width ratio, skew angle and also volume fraction and distribution of CNTs on the natural frequencies of the FG-CNTRC skew plates. Again using FSDT along with Ritz method, he focused on the free vibration analysis of FG-CNTRC rectangular plates integrated with piezoelectric layers at the bottom and top surfaces [20]. He showed that fundamental frequency of a closed circuit plate is always higher than corresponding value of a plate with open-circuit boundary conditions.

Memar et al. [21] employed TSDT and presented an isogeometric analysis for bending and free vibration analysis of CNTRC skew plates with arbitrary-oriented CNTs. They studied effect of CNT orientation on deflection and natural frequencies of the plate and found the orientation which leads to minimum or maximum values in maximum deflection and fundamental frequency of the skew plates. Employing a refined TSDT and using GDQM, Nejati et al. [22] focused on the static bending and free vibration analyses of rotating FG-CNTRC truncated conical shells. They studied effect of volume fraction, agglomeration and geometry of CNTs on the natural frequencies and static deflection of the conical shells. Fantuzzi et al. [23] used non-uniform rational B-splines (NURBS) curves and studied free vibration analysis of arbitrarily shaped FG-CNTRC plates. They focused on the influence of agglomeration on the natural frequencies. A semi-analytical solution was presented by Wang et al. [24] for free vibration analysis of FG-CNTRC doubly curved panels and shells of revolution with arbitrary boundary conditions. They studied effect of the geometrical parameters, CNTs distributions, volume fraction of CNTs as well as boundary restraint parameters on the natural frequencies. Wang et al. [25] employed FSDT and focused on the free vibration analysis of the FG-CNTRC shallow shells with arbitrary boundary conditions. They presented a comprehensive parametric investigation on the influence of elastic restraint parameters, shear deformation and rotary inertia, shallowness and material properties on the vibration characteristics of the shell. A meshless discretization technique is used by Ansari et al. [26] to present a numerical solution for free vibration analysis of FG-CNTRC elliptical plates. They modeled the plate based on the FSDT and presented various numerical results to explore the effects of concerned parameters on the natural frequencies.

Using multi-term Kantorovich–Galerkin method (MTKGM), Wang et al. [27] presented a semi-analytical solution for free vibration of symmetric sandwich plates resting on elastic foundation. They considered plate to be composed of two thin CNTRC face sheets and a thick homogenous core. They studied influence of sandwich configurations, volume fractions of CNTs, plate aspect ratio, core-to-skin thickness ratio and foundation stiffness on the natural frequencies. Zhong et al. [28] employed FSDT and presented a semi-analytical solution for free vibration analysis of FG-CNTRC circular, annular and sector plates. They presented some crucial parametric studies covering the effect of the geometrical parameters, CNTs distributions, volume fraction of CNTs and boundary conditions on the natural frequencies. Ansari et al. [29] used finite element method (FEM) and presented a numerical solution for bending and free vibration analyses of FG-CNTRC rectangular plates carrying a concentrated mass. They studied effect of boundary conditions, volume fraction and distribution of CNTs on the deflection, stress distribution and natural frequencies of the plate and effect of translational inertia of the concentrated mass on the natural frequencies of the plate. Using GDQM, Ansari et al. [30] studied free vibration analysis of arbitrary-shaped thick FG-CNTRC plates. They modeled plate based on an HSDT and reported natural frequencies for FG-CNTRC skew, quadrilateral, triangular, circular, sector and elliptical plates. Ghorbanpour Arani et al. [31, 32] used TSDT along with GDQM and studied free vibration and supersonic flutter analyses of laminated FG-CNTRC cylindrical panels. For various combinations of clamped and simple boundary conditions, they studied effects of lamination angle, number of layers, volume fractions and distributions of CNTs and geometrical parameters of the panel on the natural frequencies and critical speed of laminated FG-CNTRC panels. Using the Ritz method, Zhao et al. [33] obtained approximate values for natural frequencies of FG-CNTRC truncated conical panels with general boundary conditions. They presented a parametric study on the influence of the volume fractions of CNTs, distribution type of CNTs, boundary restraint parameters and geometrical parameters on the natural frequencies. Through a nonlinear analysis, Nguyen et al. [34] employed FSDT and presented an NURBS-based analysis for postbuckling behavior of FG-CNTRC shells. They presented some complex and useful postbuckling curves of FG-CNTRC panels and cylinders that could be useful for future references.

It can be seen that vibration analysis of CNTRC trapezoidal plates is poorly studied, especially the cantilever one which is more similar to the conditions of wings, tails and fins of aircrafts. It is due to the mathematical complexities involved in geometry of trapezoidal plates and difficulties involved in free edges. So, in this paper, free vibration analysis of cantilever FG-CNTRC trapezoidal plates are studied. The plate is modeled based on FSDT, and the set of governing equations and boundary conditions are mapped from the trapezoidal area into a rectangular one. GDQM is employed as a numerical approaches, and natural frequencies and corresponding mode shapes are reported for various cases.

2 Governing equations

As depicted in Fig. 1, an FG-CNTRC cantilever trapezoidal plate clamped at $y=0$ and free at other edges is considered. The plate is of dimensions a and b and angles α and β and is reinforced by CNTs arranged in y direction. As Fig. 2 shows, four standard patterns of distribution of CNTs are considered including UD, FG-V, FG-O and FG-X. For these types of distribution, volume fraction of CNTs is given as [35]

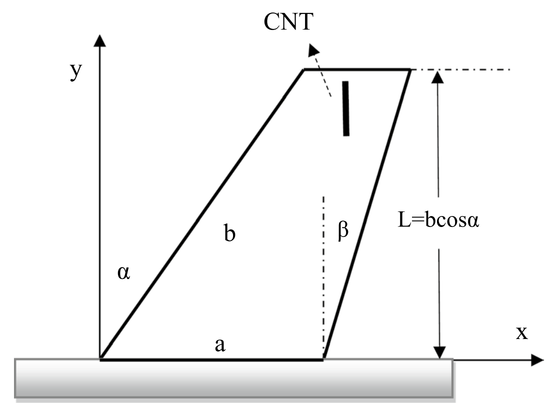

Fig. 1 Cantilever CNTRC trapezoidal plate

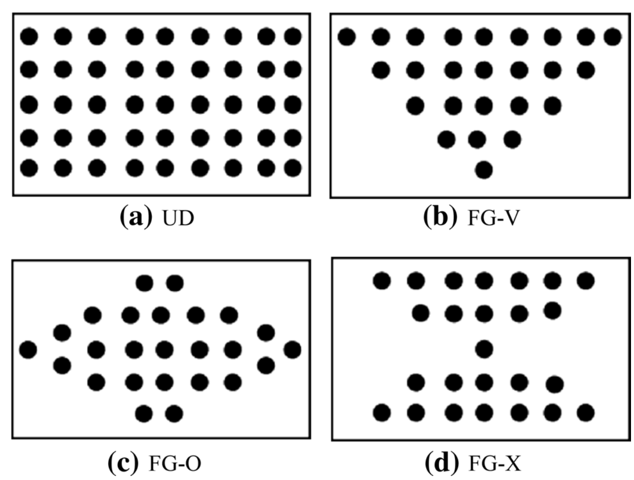

Fig. 2 Distribution patterns of CNTs

$$
\begin{aligned}
\text{UD}: &\quad V_{\mathrm{CNT}}(z) = V^*_{\mathrm{CNT}} \\
\text{FG}-V: &\quad V_{\mathrm{CNT}}(z) = \left(1+\frac{2z}{h}\right)V^*_{\mathrm{CNT}} \\
\text{FG}-O: &\quad V_{\mathrm{CNT}}(z) = 2\left(1-\frac{2|z|}{h}\right)V^*_{\mathrm{CNT}} \\
\text{FG}-X: &\quad V_{\mathrm{CNT}}(z) = 4\frac{|z|}{h}V^*_{\mathrm{CNT}}
\end{aligned}
\tag{1}
$$

where h is thickness of the plate and V^*_{CNT} is total volume fraction of CNTs which is same in all types of distribution. Also, volume fraction of isotropic matrix can be calculated as $V_{\mathrm{m}}=1-V_{\mathrm{CNT}}$. Based on the extended rule of mixture, the elastic moduli (E_{11} and E_{22}) and shear modulus (G_{12}) can be expressed as follows [36]:

$$
E_{11}(z) = \eta_1 V_{\mathrm{CNT}}(z)E^{\mathrm{CNT}}_{11} + V_{\mathrm{m}}(z)E^{\mathrm{m}} \quad \frac{\eta_2}{E_{22}(z)} = \frac{V_{\mathrm{CNT}}(z)}{E^{\mathrm{CNT}}_{22}} + \frac{V_{\mathrm{m}}(z)}{E^{\mathrm{m}}} \quad \frac{\eta_3}{G_{12}(z)} = \frac{V_{\mathrm{CNT}}(z)}{G^{\mathrm{CNT}}_{12}} + \frac{V_{\mathrm{m}}(z)}{G^{\mathrm{m}}}
\tag{2}
$$

in which E_{11}^{CNT}, E_{22}^{CNT} are elastic moduli of CNTs, G_{12}^{CNT} is shear modulus of CNT and G^{m}, and E^{m} indicate shear modulus and elastic modulus of isotropic matrix, respectively. Also, η_1, η_2 and η_3 are CNT efficiency parameters which can be calculated by matching the modulus of CNTs from the molecular dynamics (MD) results with those obtained from the rule of mixture.

Using the rule of mixture, density (ρ) and the Poisson's ratio (ν_{12}) can be calculated as [36]

$$\rho(z) = V_{\mathrm{CNT}}(z)\rho^{\mathrm{CNT}} + V_{\mathrm{m}}(z)\rho^{\mathrm{m}} \quad \upsilon_{12} = V_{\mathrm{CNT}}^{*}\upsilon_{12}^{\mathrm{CNT}} + \left(1 - V_{\mathrm{CNT}}^{*}\right)\upsilon^{\mathrm{m}} \tag{3}$$

where ν_{12}^{CNT} and ρ^{CNT} are Poisson's ratio and density of CNT, respectively, and ν^{m} and ρ^{m} are Poisson's ratio and density of matrix, respectively.

According to FSDT, the displacement field in the plate can be considered as [37, 38]

$$\begin{aligned} u_z(x,y,z) &= u(x,y) + z\psi_x(x,y) \\ v_z(x,y,z) &= v(x,y) + z\psi_y(x,y) \\ w_z(x,y,z) &= w(x,y) \end{aligned} \tag{4}$$

in which u_z, v_z and w_z are components of displacement in any desired position of the plate and u, v and w are corresponding ones at $z=0$. Also, ψ_x and ψ_y are rotation about y and x axes, respectively. Normal (ε_{ij}) and shear (γ_{ij}) components of strain can be calculated as [3]

$$\begin{Bmatrix} \varepsilon_{xx} \\ \varepsilon_{yy} \\ \gamma_{yz} \\ \gamma_{xz} \\ \gamma_{xy} \end{Bmatrix} = \begin{bmatrix} ()_{,x} & 0 & 0 & z()_{,x} & 0 \\ 0 & ()_{,y} & 0 & 0 & z()_{,y} \\ 0 & 0 & ()_{,y} & 0 & 1 \\ 0 & 0 & ()_{,x} & 1 & 0 \\ ()_{,y} & ()_{,x} & 0 & z()_{,y} & z()_{,x} \end{bmatrix} \{p\} \quad \varepsilon_{zz} = 0 \tag{5}$$

in which

$$\{p\} = \left\{ u \ v \ w \ \psi_x \ \psi_y \right\}^T \quad ()_{,x} = \frac{\partial}{\partial x} \quad ()_{,y} = \frac{\partial}{\partial y} \tag{6}$$

where superscript T indicates to transpose operator and corresponding components of stress (σ_{ij}) can be stated as follows [39]:

$$\begin{Bmatrix} \sigma_{xx} \\ \sigma_{yy} \\ \sigma_{yz} \\ \sigma_{xz} \\ \sigma_{xy} \end{Bmatrix} = \begin{bmatrix} Q_{11} & Q_{12} & 0 & 0 & 0 \\ Q_{12} & Q_{22} & 0 & 0 & 0 \\ 0 & 0 & kQ_{44} & 0 & 0 \\ 0 & 0 & 0 & kQ_{55} & 0 \\ 0 & 0 & 0 & 0 & Q_{66} \end{bmatrix} \begin{Bmatrix} \varepsilon_{xx} \\ \varepsilon_{yy} \\ \gamma_{yz} \\ \gamma_{xz} \\ \gamma_{xy} \end{Bmatrix} \tag{7}$$

where k is shear correction factor and due to the direction of CNTs, following relation should be considered for Q_{ij} [39]:

$$\begin{aligned} &Q_{11} = \frac{E_{22}}{1 - \upsilon_{12}\upsilon_{21}} \quad Q_{22} = \frac{E_{11}}{1 - \upsilon_{12}\upsilon_{21}} \quad Q_{12} = \frac{\upsilon_{12}E_{22}}{1 - \upsilon_{12}\upsilon_{21}} \\ &Q_{44} = G_{13} \quad Q_{55} = G_{23} \quad Q_{66} = G_{12} \end{aligned} \tag{8}$$

in which G_{13} and G_{23} are shear moduli and $\upsilon_{21} = \upsilon_{12}E_{22}/E_{11}$ is the Poisson's ratio.

Substituting Eq. (5) into Eq. (7), following relation can be achieved:

$$\begin{Bmatrix} \sigma_{xx} \\ \sigma_{yy} \\ \sigma_{yz} \\ \sigma_{xz} \\ \sigma_{xy} \end{Bmatrix} = \begin{bmatrix} Q_{11}()_{,x} & Q_{12}()_{,y} & 0 & zQ_{11}()_{,x} & zQ_{12}()_{,y} \\ Q_{12}()_{,x} & Q_{22}()_{,y} & 0 & zQ_{12}()_{,x} & zQ_{22}()_{,y} \\ 0 & 0 & kQ_{44}()_{,y} & 0 & kQ_{44} \\ 0 & 0 & kQ_{55}()_{,x} & kQ_{55} & 0 \\ Q_{66}()_{,y} & Q_{66}()_{,x} & 0 & zQ_{66}()_{,y} & zQ_{66}()_{,x} \end{bmatrix} \{p\} \tag{9}$$

The set of governing equations and boundary conditions can be derived using Hamilton's principle as [40]

$$\int_{t_1}^{t_2} \left(\delta T - \delta U + \delta W_{\mathrm{ext}}\right)\mathrm{d}t = 0 \tag{10}$$

in which δ is variational operator, $[t_1,t_2]$ is a desired time interval and T, U and W_{ext} are kinetic energy, potential energy and work done by external loads calculated as [31, 32]

$$\begin{aligned} U &= \frac{1}{2}\iiint_V \left(\sigma_{xx}\varepsilon_{xx} + \sigma_{yy}\varepsilon_{yy} + \sigma_{zz}\varepsilon_{zz} + \sigma_{xy}\gamma_{xy} + \sigma_{xz}\gamma_{xz} + \sigma_{yz}\gamma_{yz}\right)\mathrm{d}V \\ T &= \frac{1}{2}\iiint_V \rho\left[\left(\frac{\partial u_z}{\partial t}\right)^2 + \left(\frac{\partial v_z}{\partial t}\right)^2 + \left(\frac{\partial w_z}{\partial t}\right)^2\right]\mathrm{d}V \\ W_{ext} &= \iint_S q(x,y,t)w(x,y,t)\mathrm{d}S \end{aligned} \tag{11}$$

where V and S are volume and surface of the plate and q is the external load per unit area. Substituting Eqs. (4), (5), (7) and (11) into Eq. (10), the set of governing equations can be derived as

$$\begin{aligned} &\frac{\partial N_{xx}}{\partial x} + \frac{\partial N_{xy}}{\partial y} - I_0\frac{\partial^2 u}{\partial t^2} - I_1\frac{\partial^2 \psi_x}{\partial t^2} = 0 \\ &\frac{\partial N_{yy}}{\partial y} + \frac{\partial N_{xy}}{\partial x} - I_0\frac{\partial^2 v}{\partial t^2} - I_1\frac{\partial^2 \psi_y}{\partial t^2} = 0 \\ &\frac{\partial Q_{xz}}{\partial x} + \frac{\partial Q_{yz}}{\partial y} + q - I_0\frac{\partial^2 w}{\partial t^2} = 0 \\ &\frac{\partial M_{xx}}{\partial x} + \frac{\partial M_{xy}}{\partial y} - Q_{xz} - I_1\frac{\partial^2 u}{\partial t^2} - I_2\frac{\partial^2 \psi_x}{\partial t^2} = 0 \\ &\frac{\partial M_{yy}}{\partial y} + \frac{\partial M_{xy}}{\partial x} - Q_{yz} - I_1\frac{\partial^2 v}{\partial t^2} - I_2\frac{\partial^2 \psi_y}{\partial t^2} = 0 \end{aligned} \tag{12}$$

and external boundary conditions can be written as

$$N_{nn}\delta u_n = 0 \quad N_{ns}\delta u_s = 0 \quad Q_{nz}\delta w = 0 \quad M_{nn}\delta\psi_n = 0 \quad M_{ns}\delta\psi_s = 0 \tag{13}$$

in which

$$N_{nn}=N_{xx}n_x^2+2N_{xy}n_xn_y+N_{yy}n_y^2 \quad N_{ns}=\left(N_{yy}-N_{xx}\right)n_xn_y+N_{xy}\left(n_x^2-n_y^2\right) \quad Q_{nz}=Q_{xz}n_x+Q_{yz}n_y$$
$$M_{nn}=M_{xx}n_x^2+2M_{xy}n_xn_y+M_{yy}n_y^2 \quad M_{ns}=\left(M_{yy}-M_{xx}\right)n_xn_y+M_{xy}\left(n_x^2-n_y^2\right) \tag{14}$$

where $n_x=\cos\theta$ and $n_y=\sin\theta\theta$ are components of the normal unit vector (see Fig. 3) and components of stress resultant and inertia are defined as follows:

$$\begin{Bmatrix}N_{xx}\\N_{yy}\\N_{xy}\end{Bmatrix}=\int_{-\frac{h}{2}}^{\frac{h}{2}}\begin{Bmatrix}\sigma_{xx}\\\sigma_{yy}\\\sigma_{xy}\end{Bmatrix}\mathrm{d}z \quad \begin{Bmatrix}M_{xx}\\M_{yy}\\M_{xy}\end{Bmatrix}=\int_{-\frac{h}{2}}^{\frac{h}{2}}\begin{Bmatrix}\sigma_{xx}\\\sigma_{yy}\\\sigma_{xy}\end{Bmatrix}z\mathrm{d}z \quad \begin{Bmatrix}Q_{xz}\\Q_{yz}\end{Bmatrix}=\int_{-\frac{h}{2}}^{\frac{h}{2}}\begin{Bmatrix}\sigma_{xz}\\\sigma_{yz}\end{Bmatrix}dz \quad \begin{Bmatrix}I_0\\I_1\\I_2\end{Bmatrix}=\int_{-\frac{h}{2}}^{\frac{h}{2}}\rho\begin{Bmatrix}1\\z\\z^2\end{Bmatrix}\mathrm{d}z \tag{15}$$

Substituting Eq. (9) into Eq. (15) leads to the following relation

$$\begin{Bmatrix}N_{xx}\\N_{yy}\\N_{xy}\\M_{xx}\\M_{yy}\\M_{xy}\\Q_{yz}\\Q_{xz}\end{Bmatrix}=\begin{bmatrix}A_{11}()_{,x} & A_{12}()_{,y} & 0 & B_{11}()_{,x} & B_{12}()_{,y}\\ A_{12}()_{,x} & A_{22}()_{,y} & 0 & B_{12}()_{,x} & B_{22}()_{,y}\\ A_{66}()_{,y} & A_{66}()_{,x} & 0 & B_{66}()_{,y} & B_{66}()_{,x}\\ B_{11}()_{,x} & B_{12}()_{,y} & 0 & D_{11}()_{,x} & D_{12}()_{,y}\\ B_{12}()_{,x} & B_{22}()_{,y} & 0 & D_{12}()_{,x} & D_{22}()_{,y}\\ B_{66}()_{,y} & B_{66}()_{,x} & 0 & D_{66}()_{,y} & D_{66}()_{,x}\\ 0 & 0 & A_{44}()_{,y} & 0 & A_{44}\\ 0 & 0 & A_{55}()_{,x} & A_{55} & 0\end{bmatrix}\{p\} \tag{16}$$

in which

$$\begin{Bmatrix}A_{11}\\A_{12}\\A_{22}\\A_{66}\end{Bmatrix}=\int_{-\frac{h}{2}}^{\frac{h}{2}}\begin{Bmatrix}Q_{11}\\Q_{12}\\Q_{22}\\Q_{66}\end{Bmatrix}\mathrm{d}z \quad \begin{Bmatrix}B_{11}\\B_{12}\\B_{22}\\B_{66}\end{Bmatrix}=\int_{-\frac{h}{2}}^{\frac{h}{2}}\begin{Bmatrix}Q_{11}\\Q_{12}\\Q_{22}\\Q_{66}\end{Bmatrix}z\mathrm{d}z \quad \begin{Bmatrix}D_{11}\\D_{12}\\D_{22}\\D_{66}\end{Bmatrix}=\int_{-\frac{h}{2}}^{\frac{h}{2}}\begin{Bmatrix}Q_{11}\\Q_{12}\\Q_{22}\\Q_{66}\end{Bmatrix}z^2\mathrm{d}z \quad \begin{Bmatrix}A_{44}\\A_{55}\end{Bmatrix}=\int_{-\frac{h}{2}}^{\frac{h}{2}}k\begin{Bmatrix}Q_{44}\\Q_{55}\end{Bmatrix}\mathrm{d}z \tag{17}$$

Substituting Eq. (16) into Eq. (12) and considering $q=0$ for free vibration analysis leads to the following set of governing equations:

$$[S]\{p\}=\{0\}_{5\times1} \tag{18}$$

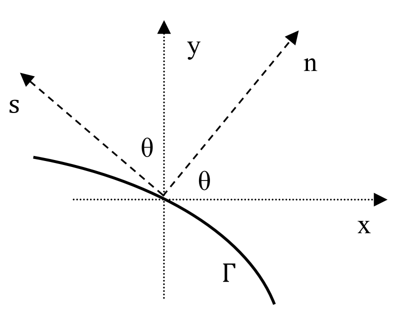

Fig. 3 n–s coordinate against Cartesian coordinate [6]

in which $S_{ij}=S_{ji}$ are presented in "Appendix 1".

Also, using Eqs. (13), (14) and (16), following relations can be written for boundary conditions:

Clamped edge ($y=0$):

$$u=0 \quad v=0 \quad w=0 \quad \psi_x=0 \quad \psi_y=0 \tag{19}$$

Free edges:

$$\begin{Bmatrix}N_{nn}\\N_{ns}\\M_{nn}\\M_{ns}\\Q_{nz}\end{Bmatrix}=[P]\{p\}=\{0\}_{5\times1} \tag{20}$$

where $[P]$ can be found in "Appendix 2"

The analysis of the non-rectangular plates uses a local parameter coordinate system rather than a Cartesian one. As shown in Fig. 4, the original trapezoidal shape of the plate in the x–y coordinates system can be mapped into a square in the ζ–η coordinates, using the following transformation [4]:

$$x=a\zeta+L\eta(\tan\alpha-G\zeta) \quad y=L\eta \tag{21}$$

in which

$$L=b\cos\alpha \quad G=\tan\alpha-\tan\beta \tag{22}$$

Applying Eq. (21) in Eq. (18) and using the method of separation of variables as

$$\begin{Bmatrix}u(\zeta,\eta,t)\\v(\zeta,\eta,t)\\w(\zeta,\eta,t)\\\psi_x(\zeta,\eta,t)\\\psi_y(\zeta,\eta,t)\end{Bmatrix}=\begin{Bmatrix}U(\zeta,\eta)\\V(\zeta,\eta)\\W(\zeta,\eta)\\X(\zeta,\eta)\\Y(\zeta,\eta)\end{Bmatrix}e^{i\Omega t} \tag{23}$$

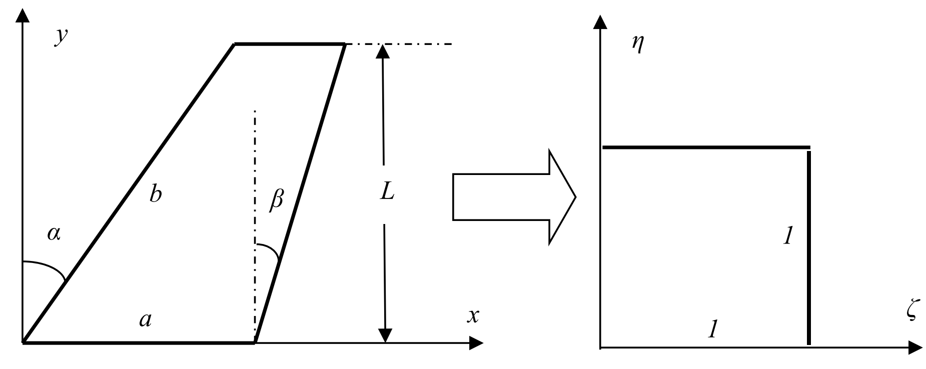

Fig. 4 Original and computational coordinates [4]

in which $i^2 = -1$ and Ω is the natural frequency, the set of equations can be rewritten as

$$[R]\{q\} = \{0\} \tag{24}$$

in which $R_{ij} = R_{ji}$ can be found in "Appendix 3" and

$$\{q\} = \{\ U\ \ V\ \ W\ \ X\ \ Y\ \}^T\ \ E = E(\eta) = \frac{1}{\phi \sec\alpha - G\eta}\ \ F = F(\zeta) = G\zeta - \tan\alpha\ \ \phi = \frac{a}{b} \tag{25}$$

Also, in a similar manner, boundary conditions can be written as

Clamped edge ($\eta = 0$):

$$U = 0\ \ V = 0\ \ W = 0\ \ X = 0\ \ Y = 0 \tag{26}$$

Free edges ($\eta = 1$, $\zeta = 0,1$)

$$[J]\{q\} = \{0\} \tag{27}$$

where $[J]$ is presented in "Appendix 4"

3 Differential quadrature method

Differential quadrature method (DQM) is one of the most popular numerical approaches which was first presented by Bellman et al. [41] in 1971. This method has been applied by many authors to present numerical solution for one-dimensional and two-dimensional problems [42–45]. Values of a two-dimensional function like $F(\zeta,\eta)$ can be expressed in a matrix form as

$$F_{ij} = F\left(\zeta_i, \eta_j\right)\ \ i = 1, 2, \dots, N\ \ j = 1, 2, \dots, M \tag{28}$$

where N and M are number of grid points in ζ and η directions, respectively. According to the differential quadrature rules, all derivatives of the function can be approximated by means of weighted linear sum of the function values at the pre-selected grid of points as [46]

$$\left[\frac{\partial^{r+s} F}{\partial \zeta^r \partial \eta^s}\right] = \left[A_\zeta^{(r)}\right][F]\left[A_\eta^{(s)}\right]^T \tag{29}$$

in which superscripts (r) and (s) indicate to order of derivation, subscripts ζ and η show derivative with respect to ζ or η, respectively. These matrices for the first-order derivatives are given as [46]:

$$\left[A_\zeta^{(1)}\right]_{in} = \begin{cases} \dfrac{\prod\limits_{\substack{k=1\\k\neq i,n}}^{N} \left(\zeta_i - \zeta_k\right)}{\prod\limits_{\substack{k=1\\k\neq n}}^{N} \left(\zeta_n - \zeta_k\right)} & i, n = 1, 2, 3, \dots, N; i \neq n \\ \sum\limits_{\substack{k=1\\k\neq i}}^{N} \dfrac{1}{\zeta_i - \zeta_k} & i = n = 1, 2, 3, \dots, N \end{cases} \quad \left[A_\eta^{(1)}\right]_{jm} = \begin{cases} \dfrac{\prod\limits_{\substack{k=1\\k\neq j,m}}^{\mathrm{m}} \left(\eta_j - \eta_k\right)}{\prod\limits_{\substack{k=1\\k\neq m}}^{\mathrm{m}} \left(\eta_{\mathrm{m}} - \eta_k\right)} & j, m = 1, 2, 3, \dots, M; j \neq m \\ \sum\limits_{\substack{k=1\\k\neq j}}^{\mathrm{m}} \dfrac{1}{\eta_j - \eta_k} & j = m = 1, 2, 3, \dots, M \end{cases} \tag{30}$$

and of higher-order derivatives are calculated as:

$$\left[A_\zeta^{(r)}\right]=\left[A_\zeta^{(1)}\right]\left[A_\zeta^{(r-1)}\right]\ \left[A_\eta^{(s)}\right]=\left[A_\eta^{(1)}\right]\left[A_\eta^{(s-1)}\right]\quad r,s=2,3,4,\ldots \tag{31}$$

For matrix $[F]_{N\times M}$, an equivalent column vector $\{\hat{F}\}_{NM\times 1}$ can be defined as [3]:

$$\hat{F}_v=F_{ij}\quad v=(j-1)N+i \tag{32}$$

and multiple of three matrices as $[a][F][b]$ can be replaced by $\left([b]^T\otimes[a]\right)\{\hat{F}\}$, in which $\otimes$ indicates the Kronecker product [3]. Thus, Eq. (29) can be rewritten as

$$\left\{\frac{\partial^{r+s}\hat{F}}{\partial\zeta^r\partial\eta^s}\right\}=\left(\left[A_\eta^{(s)}\right]\otimes\left[A_\zeta^{(r)}\right]\right)\{\hat{F}\} \tag{33}$$

In addition to number of grid points, distribution of them affects convergence of the solution. A well-accepted set of the grid points is the Gauss–Lobatto–Chebyshev points given for interval [0,1] as [46]:

$$\zeta_i=\frac{1}{2}\left\{1-\cos\left[\frac{(i-1)\pi}{N-1}\right]\right\}\ \eta_j=\frac{1}{2}\left\{1-\cos\left[\frac{(j-1)\pi}{M-1}\right]\right\} \tag{34}$$

4 DQ analog

Using DQ rules, the set of governing equation (24) can be written in the following algebraic form:

$$[K]\{s\}=\Omega^2[M]\{s\} \tag{35}$$

in which $[K]$ and $[M]$ are stiffness and mass matrices and

$$\{s\}_{5NM\times 1}=\begin{Bmatrix}\{\hat{U}\}\\\{\hat{V}\}\\\{\hat{W}\}\\\{\hat{X}\}\\\{\hat{Y}\}\end{Bmatrix} \tag{36}$$

Also, external boundary conditions (26) and (27) can be written using DQ rules as

$$[T]\{s\}=\{0\} \tag{37}$$

The grid points can be separated into two sets: boundary points which are located at the four edges of the plate and domain ones which are other interior points. By neglecting satisfying Eq. (35) at the boundary points, this equation can be written as [47]

$$\left[\bar{K}\right]\{s\}=\Omega^2\left[\bar{M}\right]\{s\} \tag{38}$$

in which bar sign implies corresponding non-square matrix. Equations (37) and (38) may be rearranged and partitioned in order to separate boundary (b) and domain (d) points as

$$\left[\bar{K}\right]_d\{s\}_d+\left[\bar{K}\right]_b\{s\}_b=\Omega^2\left(\left[\bar{M}\right]_d\{s\}_d+\left[\bar{M}\right]_b\{s\}_b\right) \tag{39.a}$$

$$[T]_d\{s\}_d+[T]_b\{s\}_b=\{0\} \tag{39.b}$$

Substituting Eq. (39.b) into Eq. (39.a) leads to the following eigen value equation:

$$\left[K^*\right]\{s\}_d=\Omega^2\left[M^*\right]\{s\}_d \tag{40}$$

in which

$$[M^*]=\left[\bar{M}\right]_d+\left[\bar{M}\right]_b[p]\ \ [K^*]=\left[\bar{K}\right]_d+\left[\bar{K}\right]_b[p] \tag{41}$$

Solving Eq. (40), values of the natural frequencies and mode shapes can be calculated as eigen values and eigen vectors, respectively. Also, mode shapes can be completed using Eq. (39.b).

5 Numerical results

In the previous section, a numerical solution was presented for free vibration analysis of FG-CNTRC cantilever trapezoidal plates. In this section, numerical results are proposed for the presented numerical solution. Unless otherwise stated, results are presented for a plate made of poly-co-vinylene (PmPV), as matrix with material properties $E^{\mathrm{m}}=2.1$ GPa, $\nu^{\mathrm{m}}=0.34$ and $\rho^{\mathrm{m}}=1150$ kg/m^3 [36] and (10,10) armchair single wall CNTs ($L=9.26$ nm, $R=0.68$ nm, $h=0.067$ nm) as the reinforcements. Elasticity moduli, shear modulus, Poisson's ratio and density of CNT at reference temperature are $E_{11}^{\mathrm{CNT}}=5.6466$ TPa, $E_{22}^{\mathrm{CNT}}=7.08$ TPa, $G_{12}^{\mathrm{CNT}}=1.9447$ TPa, $\nu_{12}^{\mathrm{CNT}}=0.175$ and $\rho^{\mathrm{CNT}}=1400$ kg/m^3 [36]. The shear moduli G_{13} and G_{23} are taken equal to G_{12} [36] and corresponding efficiency parameters are presented in Table 1 for some selected values of the total volume fraction of CNT. Also, shear correction factor is considered as $k=5/6$ [48].

First of all, convergence of the presented solution must be examined. For this purpose, consider an FG-X CNTRC trapezoidal plate of $b=1$ m, $a/b=0.75$, $h/b=0.01$, $\alpha=15°$, $\beta=-5°$ and $V_{\mathrm{CNT}}^*=0.14$. Effect of number of grid points ($N_x=N_y$) on the values of the first six natural frequencies of the plate is presented in Table 2. This table confirms

Table 1 Efficiency parameters [36]

V_{CNT}^*	η_1	$\eta_2=\eta_3$
0.11	0.149	0.934
0.14	0.150	0.941
0.17	0.149	1.381

Table 2 Convergence of the presented numerical solution ($b=1$ m, $a/b=0.75$, $h/b=0.01$, $\alpha=15°$, $\beta=-5°$, $V^*_{CNT}=0.14$)

N	Natural frequencies (Hz)					
	Ω_1	Ω_2	Ω_3	Ω_4	Ω_5	Ω_6
11	24.83263	34.51617	83.62336	132.5699	136.0458	157.3429
13	24.13631	34.44771	80.71520	132.4562	135.8034	157.4896
15	23.82860	34.45238	79.67155	132.4433	135.6308	157.7460
17	23.68160	34.46073	79.22733	132.4456	135.5714	157.9443
19	23.60707	34.45913	79.02393	132.4474	135.5601	158.0784
21	23.56823	34.45240	78.92684	132.4474	135.5577	158.1593
23	23.54815	34.44595	78.87908	132.4462	135.5542	158.2013
25	23.53817	34.44170	78.85541	132.4449	135.5503	158.2198

Table 3 Natural frequencies of a homogenous trapezoidal plate ($E_{11}=E_{22}=68.2$ Gpa, $\nu_{12}=\nu_{21}=0.35$, $\rho=2860$ kg/m^3, $a=8.8$ cm, $b=10.35$ cm, $h=0.98$ mm, $\alpha=27°$, $\beta=-13°$)

	Natural frequencies (Hz)					
	Ω_1	Ω_2	Ω_3	Ω_4	Ω_5	Ω_6
Presented solution	151.8647	579.7707	676.2399	1493.146	1734.581	2288.901
DQM (Torabi et al. [7])	153.1031	579.5874	676.4468	1492.844	1735.459	2291.540
Experimental results [49]	153.0000	594.0000	717.0000	1571.000	1970.000	2320.000

convergence of the presented solution, and $N_x=N_y=19$ is considered in all of the following examples.

In order to confirm accuracy of the presented solution, a homogenous trapezoidal plate of $E_{11}=E_{22}=68.2$ GPa, $\nu_{12}=\nu_{21}=0.35$, $\rho=2860$ kg/m^3, $a=8.8$ cm, $b=10.35$ cm, $h=0.98$ mm, $\alpha=27°$ and $\beta=-13°$ is considered. Table 3 shows values of the first six natural frequencies of the plate and corresponding ones presented by other researchers. A comparison between results confirms high accuracy of the presented solution. Also corresponding mode shapes are depicted in Fig. 5 which show accuracy of the presented solution.

An UD CNTRC square plate of $h/b=0.02$ and $V^*_{CNT}=0.14$ is considered. In Table 4, dimensionless values ($\lambda=\Omega b^2\sqrt{\rho^m/E^m}\Big/h$) of the first eight natural frequencies are reported and are compared with numerical ones reported by Memar et al. [21]. As this table shows, results are in good agreement and the small difference can be explained by difference in employed theories which is FSDT in the presented paper and TSDT in Ref. [21]. Also, in Fig. 6, corresponding mode shapes are depicted against corresponding ones reported by Memar et al. [21] which reveals high accuracy of the presented numerical solution.

Consider an FG-CNTRC trapezoidal plate of $b=1$ m, $a/b=0.7$, $h/b=0.02$, $\alpha=15°$ and $\beta=-15°$. For various values of volume fraction of CNTs and different types of distribution, Table 5 presents values of the first six natural frequencies in Hz. This table shows that using CNTs leads to considerable increase in all natural frequencies and increase in value of the volume fraction of CNTs increases all natural frequencies as well. It can be explained by high values of elastic and shear moduli of CNTs. Table 5 also shows that types of distribution of CNTs can be sorted in order of increase in natural frequencies as FG-X, UD, FG-V and FG-O which is in agreement with those reported by other authors for free vibration analysis of FG-CNTRC plates and shells [19, 31]. It is worth mentioning that results of Table 5 may serve as benchmarks for future studies.

An FG-X CNTRC trapezoidal plate of $V^*_{CNT}=0.11$, $b=1$ m, $a/b=0.75$ and $h/b=0.02$ is chosen. Effect of angles α and β on the natural frequencies of the first six modes are depicted in Fig. 7. As shown in this figure, increase in values of α increases all natural frequencies and in order to achieve higher natural frequencies it is better to use negative value of β. Big positive values of α and big negative values of β decreases width (mass) of the plate at unsupported areas and makes the plate more similar to a triangle which leads to rise in all natural frequencies.

Because of opposite effects of α and positive values of β on values of the natural frequencies of trapezoidal plates, it can be interesting to study effect of skew angles on natural frequencies of FG-CNTRC skew plates. For this purpose, consider an FG-X CNTRC skew plate ($\alpha=\beta$) of $b=1$ m, $a/b=0.25$ and $h/b=0.01$. For various values of $\alpha=\beta$ and volume fraction of CNTs, Table 6 presents values of the first six natural frequencies. This table shows that no specified trend can be detected for effect of skew angle on value of natural frequencies of the plate which can be explained by confrontation between effects of α and β.

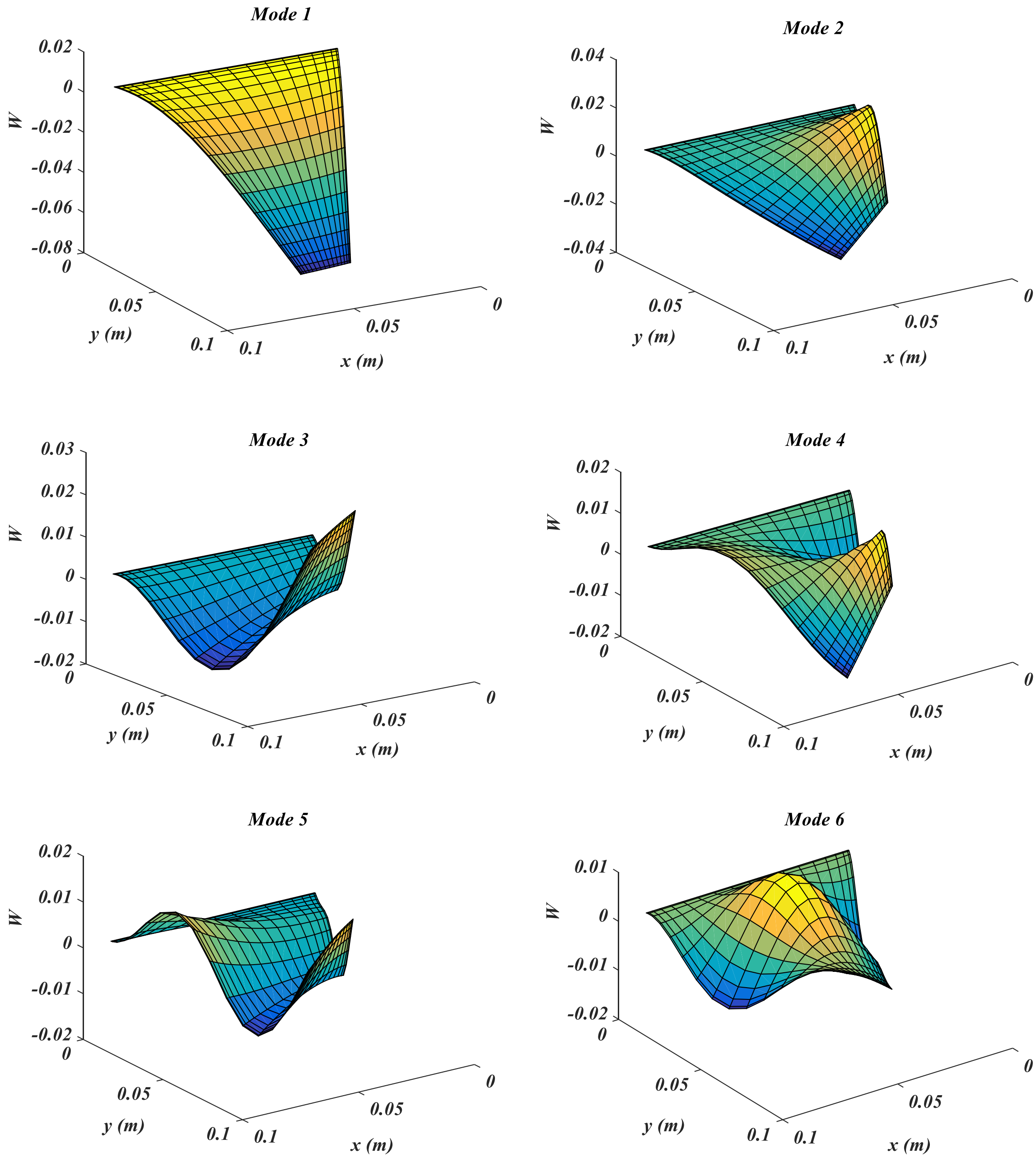

Fig. 5 First six mode shapes of a homogenous trapezoidal plate ($E=68.2$ Gpa, $\nu=0.35$, $\rho=2860$ kg/m^3, $a=8.8$ cm, $b=10.35$ cm, $h=0.98$ mm, $\alpha=27°$, $\beta=-13°$)

Table 4 Dimensionless natural frequencies of an UD CNTRC square plate ($h/b=0.02$, $V^*_{CNT}=0.14$)

	Dimensionless natural frequencies $\left(\lambda = \Omega b^2 \sqrt{\rho^m / E^m} \Big/ h\right)$							
	λ_1	λ_2	λ_3	λ_4	λ_5	λ_6	λ_7	λ_8
Present	7.482	7.913	11.233	21.096	37.653	43.652	44.107	46.066
Memar et al. [21]	7.479	7.908	11.235	21.087	37.646	43.674	44.126	46.099

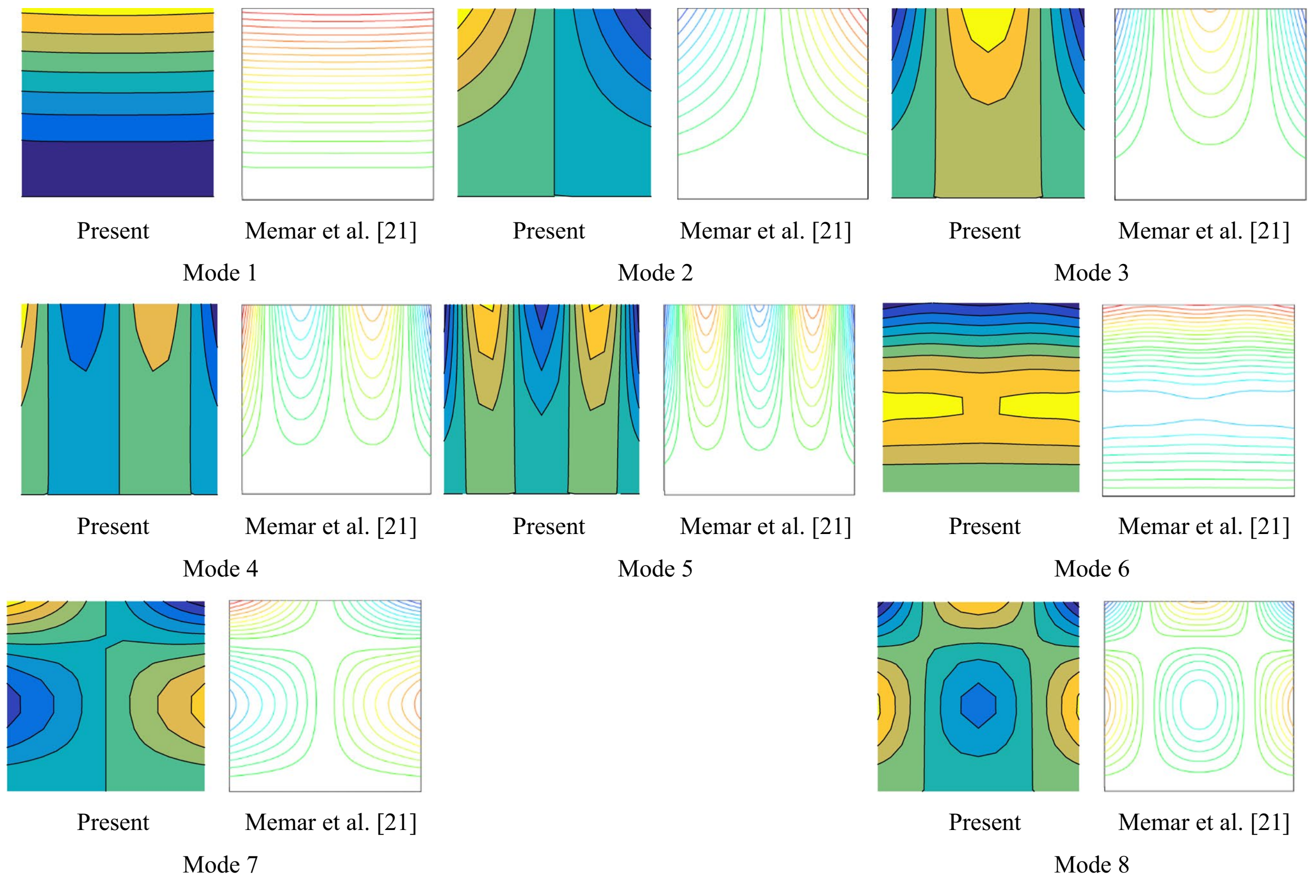

Fig. 6 First eight mode shapes of an UD CNTRC square plate ($h/b=0.02$, $V^*_{CNT}=0.14$)

Table 5 Effect of distribution and volume fraction of CNTs on the natural frequencies of an FG-CNTRC trapezoidal plate ($b=1$ m, $a/b=0.7$, $h/b=0.02$, $\alpha=15°$, $\beta=-15°$)

V^*_{CNT}	Distribution pattern	Natural frequencies (Hz)					
		Ω_1	Ω_2	Ω_3	Ω_4	Ω_5	Ω_6
0	UD	6.907254	33.63638	35.51616	87.02458	90.09614	157.8853
	FG-V	6.907254	33.63638	35.51616	87.02458	90.09614	157.8853
	FG-O	6.907254	33.63638	35.51616	87.02458	90.09614	157.8853
	FG-X	6.907254	33.63638	35.51616	87.02458	90.09614	157.8853
0.11	UD	40.56566	80.76841	181.1958	233.3481	241.8614	399.9144
	FG-V	34.15201	72.38557	156.7862	208.8734	226.1778	270.5313
	FG-O	29.83221	65.51283	138.8090	189.0453	211.0150	336.1000
	FG-X	48.53877	92.36501	208.8705	264.3048	266.9876	432.9294
0.14	UD	45.16049	87.48807	197.8984	252.0496	256.6066	419.9638
	FG-V	38.00395	78.12257	172.3735	225.6385	238.7661	276.3044
	FG-O	33.20877	70.36550	153.0207	203.8370	221.1887	360.7189
	FG-X	54.03495	100.5511	226.8374	285.5655	285.7629	456.8818
0.17	UD	50.00738	100.0463	224.0140	289.0974	300.5069	497.6425
	FG-V	41.95668	89.60738	193.1475	258.472	281.6912	339.9825
	FG-O	36.59960	80.51910	170.5655	232.5961	259.9196	413.9974
	FG-X	60.05115	115.3790	260.2737	330.0358	335.3878	546.6670

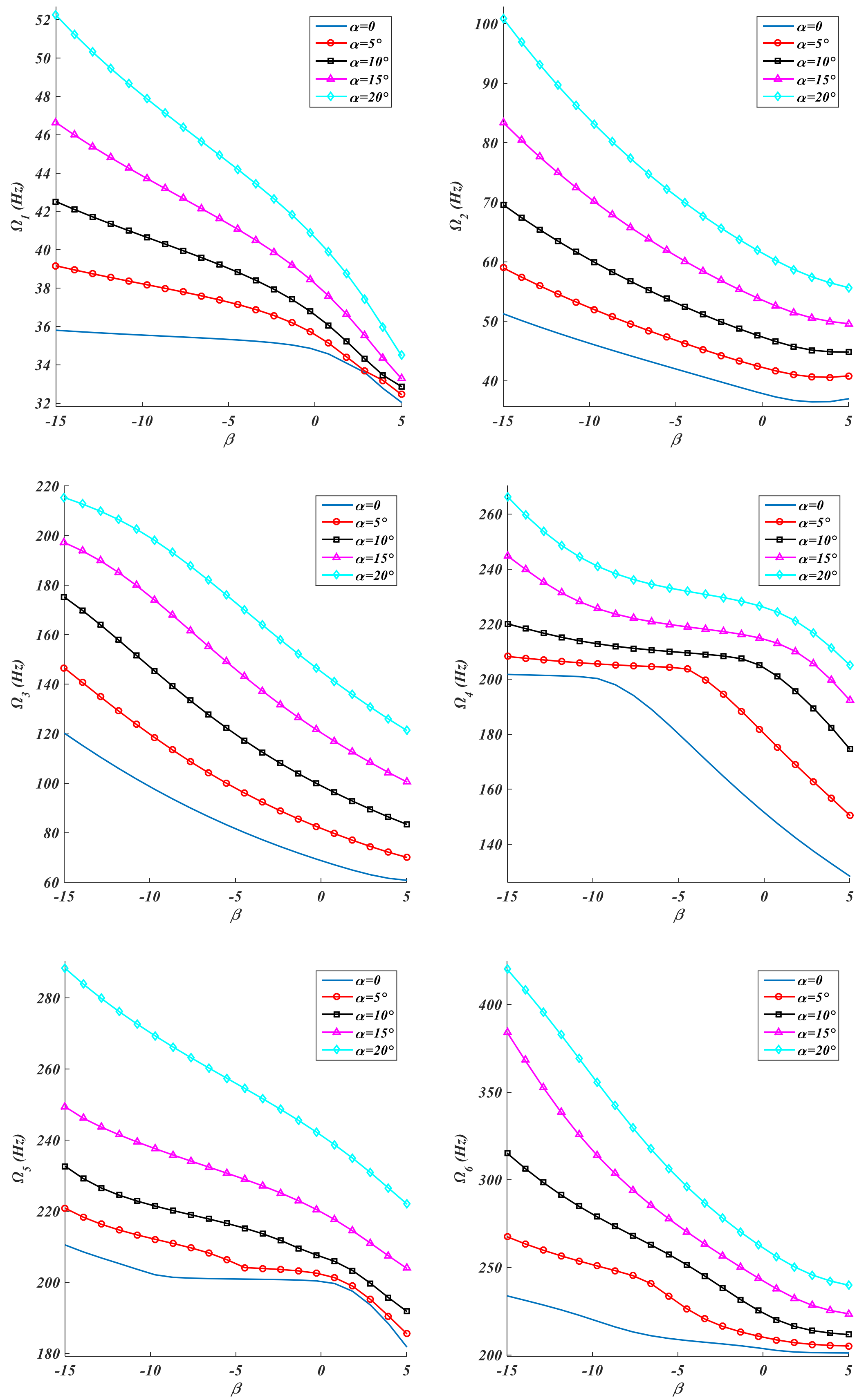

Fig. 7 Effect of angles α and β of CNTs on the natural frequencies of an FG-CNTRC trapezoidal plate (FG-X, $V^*_{CNT}=0.11$, $b=1$ m, $a/b=0.75$, $h/b=0.02$)

Table 6 Effect of skew angle on the natural frequencies of an FG-CNTRC skew plate for various values of volume fraction (FG-X, $b=1$ m, $a/b=0.25$, $h/b=0.01$)

V^*_{CNT}	α	Natural frequencies (Hz)					
		Ω_1	Ω_2	Ω_3	Ω_4	Ω_5	Ω_6
0	0	2.223800	13.91496	17.45577	39.02661	54.04806	76.76280
	5	2.232650	13.89768	17.55369	39.01026	54.28713	76.61938
	10	2.238962	13.89165	17.82912	38.96200	55.10369	76.32405
	15	2.254437	13.88504	18.28849	38.91201	56.43882	75.93666
	20	2.278217	13.89358	18.93256	38.89236	58.31103	75.58087
0.11	0	17.60115	28.16587	107.7704	122.9058	235.6413	281.2692
	5	14.99881	31.40316	98.79637	124.0130	240.0856	251.1562
	10	11.50442	36.40242	84.08418	123.1521	214.4974	247.3623
	15	8.890742	38.09930	74.32749	115.0675	190.6047	238.5399
	20	7.693624	34.47309	70.39124	101.9006	176.6449	214.0843
0.14	0	19.80917	30.16614	120.7018	135.0358	242.7974	293.3443
	5	16.58932	34.02706	109.3184	136.2334	248.2942	267.3207
	10	12.52594	39.60807	91.65889	134.5290	228.4604	259.1383
	15	9.570982	41.13884	80.37558	124.2513	202.5349	253.7213
	20	8.313955	36.60245	75.74266	108.7883	187.2720	227.3000
0.17	0	21.68846	35.49964	132.9152	152.9945	302.0099	357.8986
	5	18.61875	39.38257	122.4377	154.3641	307.1703	316.1768
	10	14.38445	45.55224	104.8752	153.6245	270.255	314.1168
	15	11.16566	47.80778	93.09015	144.2107	240.5565	300.7031
	20	9.643494	43.56260	88.40120	128.3157	223.2372	270.2151

Consider a UD CNTRC trapezoidal plate of $V^*_{CNT}=0.17$, $b=1$ m, $\alpha=15°$ and $\beta=-5°$. Effect of thickness ratio (h/b) and aspect ratio (a/b) on the first six natural frequencies of the plate are depicted in Fig. 8. As shown in this figure, increase in thickness of the plate leads to rise in all natural frequencies of the plate which shows more increase in stiffness of the plate in comparison with its inertia. This figure also shows that increase in width of the plate decreases all natural frequencies intensively. Increase in width of the plate increases inertia and decreases stiffness of the plate which decreases all natural frequencies.

As depicted in Fig. 8, smooth decrease can be seen for variation of the first three modes of the plate versus variation of aspect ratio; but for specified values of aspect ratio ($a/b=0.87$ and $a/b=1.136$), some sudden changes can be seen in fourth, fifth and sixth modes. Figure 9 shows variation of natural frequencies of modes 4–6 simultaneously. This figure reveals that for $a/b=0.87$ and $a/b=1.136$, sequence of mode changes and it is the main reason of those sudden changes.

6 Conclusions

Using GDQM, a numerical solution was presented for free vibration analysis of cantilever FG-CNTRC trapezoidal plates. The plate was modeled based on FSDT, and effective mechanical properties were calculated using extended rule of mixture. Convergence and accuracy of the presented numerical solution were confirmed, and effect of geometrical parameters and volume fraction and distribution of CNTs on the natural frequencies of the plate were studied through numerical examples. Numerical results showed that adding CNTs to cantilever trapezoidal plates leads to considerable rise in all natural frequencies and in order to increase natural frequencies it is better to increase volume fraction of CNTs and using FG-X pattern for distribution of CNTs. Numerical examples showed that increase in thickness of the plate leads to increase in natural frequencies but increase in width of the plate decreases all natural frequencies and may change sequence of modes. It was shown by numerical results that all natural frequencies increases by decreasing width of the plate at the unsupported parts of the plate located near the outer free edge.

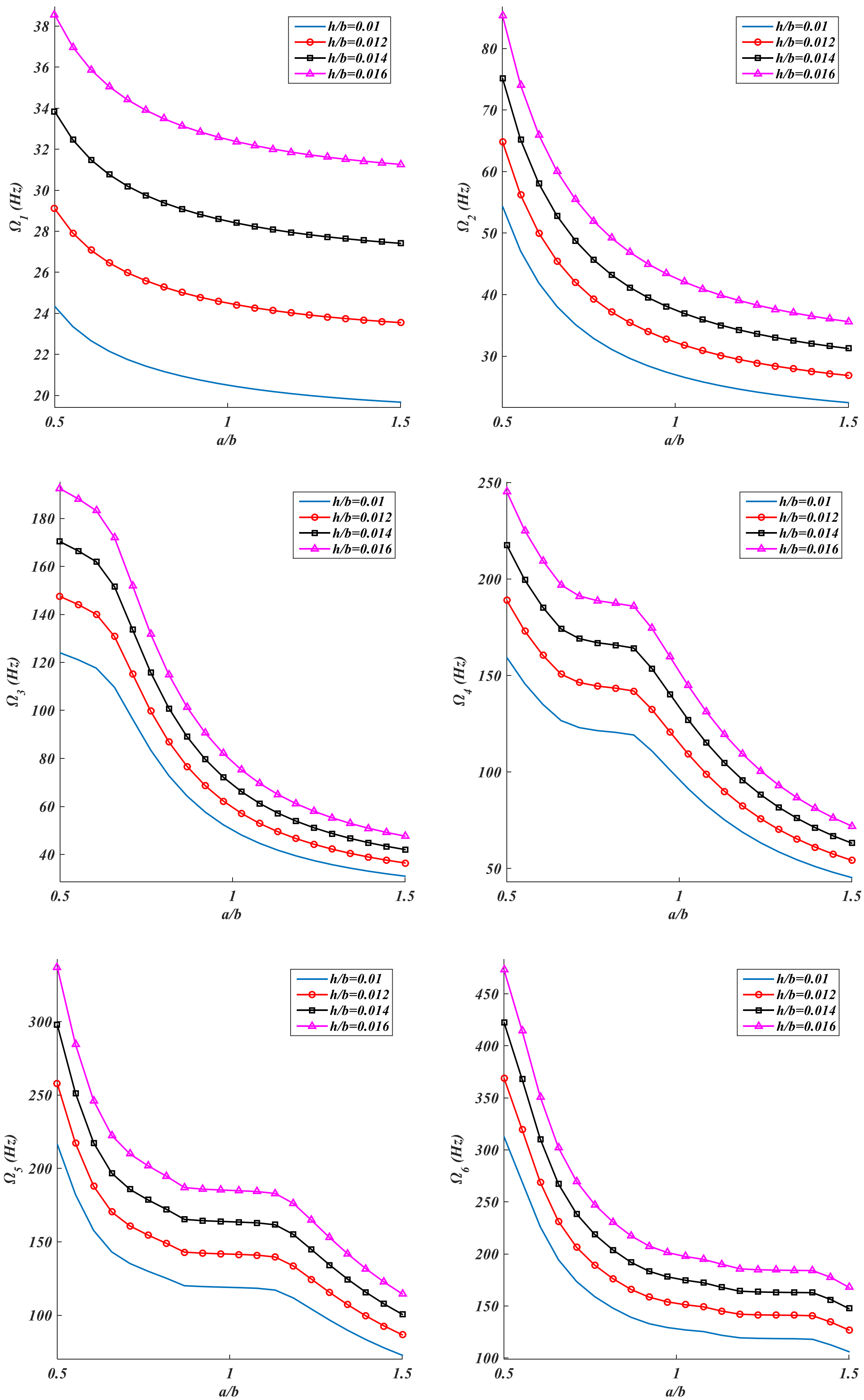

Fig. 8 Effect of thickness and aspect ratio on the natural frequencies of an FG-CNTRC trapezoidal plate (UD, $V^*_{CNT}=0.17$, $b=1$ m, $\alpha=15°$ and $\beta=-5°$)

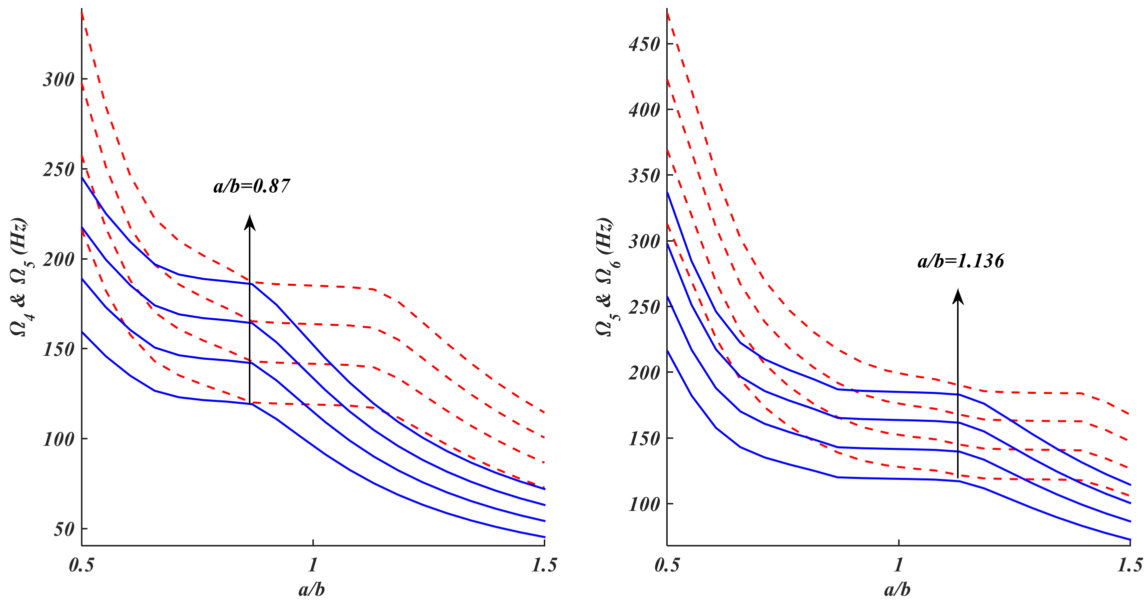

Fig. 9 Effect of aspect ratio on sequence of modes

Appendix 1

$$
\begin{array}{lll}
S_{11}=A_{11}\frac{\partial^2}{\partial x^2}+A_{66}\frac{\partial^2}{\partial y^2}-I_0\frac{\partial^2}{\partial t^2} & S_{12}=\left(A_{12}+A_{66}\right)\frac{\partial^2}{\partial x\partial y} & S_{13}=0\\
S_{14}=B_{11}\frac{\partial^2}{\partial x^2}+B_{66}\frac{\partial^2}{\partial y^2}-I_1\frac{\partial^2}{\partial t^2} & S_{15}=\left(B_{12}+B_{66}\right)\frac{\partial^2}{\partial x\partial y} & S_{22}=A_{66}\frac{\partial^2}{\partial x^2}+A_{22}\frac{\partial^2}{\partial y^2}-I_0\frac{\partial^2}{\partial t^2}\\
S_{23}=0 & S_{24}=\left(B_{12}+B_{66}\right)\frac{\partial^2}{\partial x\partial y} & S_{25}=B_{66}\frac{\partial^2}{\partial x^2}+B_{22}\frac{\partial^2}{\partial y^2}-I_1\frac{\partial^2}{\partial t^2}\\
S_{33}=-A_{55}\frac{\partial^2}{\partial x^2}-A_{44}\frac{\partial^2}{\partial y^2}+I_0\frac{\partial^2}{\partial t^2} & S_{34}=-A_{55}\frac{\partial}{\partial x} & S_{35}=-A_{44}\frac{\partial}{\partial y}\\
S_{44}=D_{11}\frac{\partial^2}{\partial x^2}+D_{66}\frac{\partial^2}{\partial y^2}-A_{55}-I_2\frac{\partial^2}{\partial t^2} & S_{45}=\left(D_{12}+D_{66}\right)\frac{\partial^2}{\partial x\partial y} & S_{55}=D_{66}\frac{\partial^2}{\partial x^2}+D_{22}\frac{\partial^2}{\partial y^2}-A_{44}-I_2\frac{\partial^2}{\partial t^2}
\end{array}
\tag{42}
$$

Appendix 2

$$
\begin{array}{ll}
P_{11}=\left(n_x^2A_{11}+n_y^2A_{12}\right)()_{,x}+2n_xn_yA_{66}()_{,y} & P_{21}=n_xn_y\left(A_{12}-A_{11}\right)()_{,x}+\left(n_x^2-n_y^2\right)A_{66}()_{,y}\\
P_{12}=2n_xn_yA_{66}()_{,x}+\left(n_x^2A_{12}+n_y^2A_{22}\right)()_{,y} & P_{22}=\left(n_x^2-n_y^2\right)A_{66}()_{,x}+n_xn_y\left(A_{22}-A_{12}\right)()_{,y}\\
P_{13}=0 & P_{23}=0\\
P_{14}=\left(n_x^2B_{11}+n_y^2B_{12}\right)()_{,x}+2n_xn_yB_{66}()_{,y} & P_{24}=n_xn_y\left(B_{12}-B_{11}\right)()_{,x}+\left(n_x^2-n_y^2\right)B_{66}()_{,y}\\
P_{15}=2n_xn_yB_{66}()_{,x}+\left(n_x^2B_{12}+n_y^2B_{22}\right)()_{,y} & P_{25}=\left(n_x^2-n_y^2\right)B_{66}()_{,x}+n_xn_y\left(B_{22}-B_{12}\right)()_{,y}\\
P_{31}=\left(n_x^2B_{11}+n_y^2B_{12}\right)()_{,x}+2n_xn_yB_{66}()_{,y} & P_{41}=n_xn_y\left(B_{12}-B_{11}\right)()_{,x}+\left(n_x^2-n_y^2\right)B_{66}()_{,y}\\
P_{32}=2n_xn_yB_{66}()_{,x}+\left(n_x^2B_{12}+n_y^2B_{22}\right)()_{,y} & P_{42}=\left(n_x^2-n_y^2\right)B_{66}()_{,x}+n_xn_y\left(B_{22}-B_{12}\right)()_{,y}\\
P_{33}=0 & P_{43}=0\\
P_{34}=\left(n_x^2D_{11}+n_y^2D_{12}\right)()_{,x}+2n_xn_yD_{66}()_{,y} & P_{44}=n_xn_y\left(D_{12}-D_{11}\right)()_{,x}+\left(n_x^2-n_y^2\right)D_{66}()_{,y}\\
P_{35}=2n_xn_yD_{66}()_{,x}+\left(n_x^2D_{12}+n_y^2D_{22}\right)()_{,y} & P_{45}=\left(n_x^2-n_y^2\right)D_{66}()_{,x}+n_xn_y\left(D_{22}-D_{12}\right)()_{,y}\\
P_{51}=0 \quad P_{52}=0 \quad P_{53}=n_xA_{55}()_{,x}+n_yA_{44}()_{,y} & P_{54}=n_xA_{55}()_{,x} \quad P_{55}=n_yA_{44}()_{,y}
\end{array}
\tag{43}
$$

Appendix 3

$$
\begin{aligned}
&R_{11} = \left(A_{11} + A_{66}F^2\right)E^2\frac{\partial^2}{\partial\zeta^2} + A_{66}\left(2FE\frac{\partial^2}{\partial\zeta\partial\eta} + \frac{\partial^2}{\partial\eta^2} + 2GFE^2\frac{\partial}{\partial\zeta}\right) + \Omega^2 I_0 L^2\\
&R_{12} = \left(A_{12} + A_{66}\right)\left(FE^2\frac{\partial^2}{\partial\zeta^2} + E\frac{\partial^2}{\partial\zeta\partial\eta} + GE^2\frac{\partial}{\partial\zeta}\right) \quad R_{13} = 0\\
&R_{14} = \left(B_{11} + B_{66}F^2\right)E^2\frac{\partial^2}{\partial\zeta^2} + B_{66}\left(2FE\frac{\partial^2}{\partial\zeta\partial\eta} + \frac{\partial^2}{\partial\eta^2} + 2GFE^2\frac{\partial}{\partial\zeta}\right) + \Omega^2 I_1 L^2\\
&R_{15} = \left(B_{12} + B_{66}\right)\left(FE^2\frac{\partial^2}{\partial\zeta^2} + E\frac{\partial^2}{\partial\zeta\partial\eta} + GE^2\frac{\partial}{\partial\zeta}\right)\\
&R_{22} = \left(A_{66} + A_{22}F^2\right)E^2\frac{\partial^2}{\partial\zeta^2} + A_{22}\left(2FE\frac{\partial^2}{\partial\zeta\partial\eta} + \frac{\partial^2}{\partial\eta^2} + 2GFE^2\frac{\partial}{\partial\zeta}\right) + \Omega^2 I_0 L^2\\
&R_{23} = 0 \quad R_{24} = \left(B_{12} + B_{66}\right)\left(FE^2\frac{\partial^2}{\partial\zeta^2} + E\frac{\partial^2}{\partial\zeta\partial\eta} + GE^2\frac{\partial}{\partial\zeta}\right)\\
&R_{25} = \left(B_{66} + B_{22}F^2\right)E^2\frac{\partial^2}{\partial\zeta^2} + B_{22}\left(2FE\frac{\partial^2}{\partial\zeta\partial\eta} + \frac{\partial^2}{\partial\eta^2} + 2GFE^2\frac{\partial}{\partial\zeta}\right) + \Omega^2 I_1 L^2\\
&R_{33} = -\left(A_{55} + A_{44}F^2\right)E^2\frac{\partial^2}{\partial\zeta^2} - A_{44}\left(2FE\frac{\partial^2}{\partial\zeta\partial\eta} + \frac{\partial^2}{\partial\eta^2} + 2GFE^2\frac{\partial}{\partial\zeta}\right) - \Omega^2 I_0 L^2\\
&R_{34} = -A_{55}LE\frac{\partial}{\partial\zeta} \quad R_{35} = -A_{44}L\left(FE\frac{\partial}{\partial\zeta} + \frac{\partial}{\partial\eta}\right)\\
&R_{44} = \left(D_{11} + D_{66}F^2\right)E^2\frac{\partial^2}{\partial\zeta^2} + D_{66}\left(2FE\frac{\partial^2}{\partial\zeta\partial\eta} + \frac{\partial^2}{\partial\eta^2} + 2GFE^2\frac{\partial}{\partial\zeta}\right) - A_{55}L^2 + \Omega^2 I_2 L^2\\
&R_{45} = \left(D_{12} + D_{66}\right)\left(FE^2\frac{\partial^2}{\partial\zeta^2} + E\frac{\partial^2}{\partial\zeta\partial\eta} + GE^2\frac{\partial}{\partial\zeta}\right)\\
&R_{55} = \left(D_{66} + D_{22}F^2\right)E^2\frac{\partial^2}{\partial\zeta^2} + D_{22}\left(2FE\frac{\partial^2}{\partial\zeta\partial\eta} + \frac{\partial^2}{\partial\eta^2} + 2GFE^2\frac{\partial}{\partial\zeta}\right) - A_{44}L^2 + \Omega^2 I_2 L^2
\end{aligned}
\tag{44}
$$

Appendix 4

$$
\begin{aligned}
&J_{11} = \left(n_x^2 A_{11} + n_y^2 A_{12} + 2n_x n_y A_{66} F\right) E()_{,\zeta} + 2n_x n_y A_{66}()_{,\eta} \\
&J_{12} = \left[\left(n_x^2 A_{12} + n_y^2 A_{22}\right) F + 2n_x n_y A_{66}\right] E()_{,\zeta} + \left(n_x^2 A_{12} + n_y^2 A_{22}\right)()_{,\eta} \\
&J_{13} = 0 \\
&J_{14} = \left(n_x^2 B_{11} + n_y^2 B_{12} + 2n_x n_y B_{66} F\right) E()_{,\zeta} + 2n_x n_y B_{66}()_{,\eta} \\
&J_{15} = \left[\left(n_x^2 B_{12} + n_y^2 B_{22}\right) F + 2n_x n_y B_{66}\right] E()_{,\zeta} + \left(n_x^2 B_{12} + n_y^2 B_{22}\right)()_{,\eta} \\
&J_{21} = \left[n_x n_y \left(A_{12} - A_{11}\right) + \left(n_x^2 - n_y^2\right) A_{66} F\right] E()_{,\zeta} + \left(n_x^2 - n_y^2\right) A_{66}()_{,\eta} \\
&J_{22} = \left[n_x n_y \left(A_{22} - A_{12}\right) F + \left(n_x^2 - n_y^2\right) A_{66}\right] E()_{,\zeta} + n_x n_y \left(A_{22} - A_{12}\right)()_{,\eta} \\
&J_{23} = 0 \\
&J_{24} = \left[n_x n_y \left(B_{12} - B_{11}\right) + \left(n_x^2 - n_y^2\right) B_{66} F\right] E()_{,\zeta} + \left(n_x^2 - n_y^2\right) B_{66}()_{,\eta} \\
&J_{25} = \left[n_x n_y \left(B_{22} - B_{12}\right) F + \left(n_x^2 - n_y^2\right) B_{66}\right] E()_{,\zeta} + n_x n_y \left(B_{22} - B_{12}\right)()_{,\eta} \\
&J_{31} = \left(n_x^2 B_{11} + n_y^2 B_{12} + 2n_x n_y B_{66} F\right) E()_{,\zeta} + 2n_x n_y B_{66}()_{,\eta} \\
&J_{32} = \left[\left(n_x^2 B_{12} + n_y^2 B_{22}\right) F + 2n_x n_y B_{66}\right] E()_{,\zeta} + \left(n_x^2 B_{12} + n_y^2 B_{22}\right)()_{,\eta} \\
&J_{33} = 0 \\
&J_{34} = \left(n_x^2 D_{11} + n_y^2 D_{12} + 2n_x n_y D_{66} F\right) E()_{,\zeta} + 2n_x n_y D_{66}()_{,\eta} \\
&J_{35} = \left[\left(n_x^2 D_{12} + n_y^2 D_{22}\right) F + 2n_x n_y D_{66}\right] E()_{,\zeta} + \left(n_x^2 D_{12} + n_y^2 D_{22}\right)()_{,\eta} \\
&J_{41} = \left[n_x n_y \left(B_{12} - B_{11}\right) + \left(n_x^2 - n_y^2\right) B_{66} F\right] E()_{,\zeta} + \left(n_x^2 - n_y^2\right) B_{66}()_{,\eta} \\
&J_{42} = \left[n_x n_y \left(B_{22} - B_{12}\right) F + \left(n_x^2 - n_y^2\right) B_{66}\right] E()_{,\zeta} + n_x n_y \left(B_{22} - B_{12}\right)()_{,\eta} \\
&J_{43} = 0 \\
&J_{44} = \left[n_x n_y \left(D_{12} - D_{11}\right) + \left(n_x^2 - n_y^2\right) D_{66} F\right] E()_{,\zeta} + \left(n_x^2 - n_y^2\right) D_{66}()_{,\eta} \\
&J_{45} = \left[n_x n_y \left(D_{22} - D_{12}\right) F + \left(n_x^2 - n_y^2\right) D_{66}\right] E()_{,\zeta} + n_x n_y \left(D_{22} - D_{12}\right)()_{,\eta} \\
&J_{51} = 0 \quad J_{52} = 0 \quad J_{53} = \left(n_x A_{55} + n_y A_{44} F\right) E()_{,\zeta} + n_y A_{44}()_{,\eta} \quad J_{54} = n_x A_{55} L \quad J_{55} = n_y A_{44} L \\
&()_{,\zeta} = \frac{\partial}{\partial \zeta} ()_{,\eta} = \frac{\partial}{\partial \eta} C
\end{aligned}
\tag{45}
$$

References

1. Iijima S (1991) Helical microtubules of graphitic carbon. Nature 354:56–58
2. Afshari H, Torabi K (2017) A Parametric study on flutter analysis of cantilevered trapezoidal FG sandwich plates. AUT J Mech Eng 1:191–210
3. Torabi K, Afshari H (2016) Optimization for flutter boundaries of cantilevered trapezoidal thick plates. J Braz Soc Mech Sci Eng 39:1545–1561
4. Torabi K, Afshari H (2016) Generalized differential quadrature method for vibration analysis of cantilever trapezoidal FG thick plate. J Solid Mech 8:184–203
5. Torabi K, Afshari H (2017) Optimization of flutter boundaries of cantilevered trapezoidal functionally graded sandwich plates. J Sandwich Struct Mater 21:503–531
6. Torabi K, Afshari H (2017) Vibration analysis of a cantilevered trapezoidal moderately thick plate with variable thickness. Eng Solid Mech 5:71–92

7. Torabi K, Afshari H, Aboutalebi FH (2019) Vibration and flutter analyses of cantilever trapezoidal honeycomb sandwich plates. J Sandwich Struct Mater 21:109963621772874
8. Zhu P, Lei ZX, Liew KM (2012) Static and free vibration analyses of carbon nanotube-reinforced composite plates using finite element method with first order shear deformation plate theory. Compos Struct 94:1450–1460
9. Zhang LW, Lei ZX, Liew KM (2015) Free vibration analysis of functionally graded carbon nanotube-reinforced composite triangular plates using the FSDT and element-free IMLS-Ritz method. Compos Struct 120:189–199
10. Zhang LW, Lei ZX, Liew KM (2015) Vibration characteristic of moderately thick functionally graded carbon nanotube reinforced composite skew plates. Compos Struct 122:172–183
11. Zhang LW, Zhang Y, Zou GL, Liew KM (2016) Free vibration analysis of triangular CNT-reinforced composite plates subjected to in-plane stresses using FSDT element-free method. Compos Struct 149:247–260
12. Lei ZX, Zhang LW, Liew KM (2016) Vibration of FG-CNT reinforced composite thick quadrilateral plates resting on Pasternak foundations. Eng Anal Boundary Elem 64:1–11
13. García-Macías E, Castro-Triguero R, Saavedra Flores EI, Friswell MI, Gallego R (2016) Static and free vibration analysis of functionally graded carbon nanotube reinforced skew plates. Compos Struct 140:473–490
14. Lei ZX, Zhang LW, Liew KM (2015) Free vibration analysis of laminated FG-CNT reinforced composite rectangular plates using the kp-Ritz method. Compos Struct 127:245–259
15. Guo XY, Zhang W (2016) Nonlinear vibrations of a reinforced composite plate with carbon nanotubes. Compos Struct 135:96–108
16. Selim BA, Zhang LW, Liew KM (2016) Vibration analysis of CNT reinforced functionally graded composite plates in a thermal environment based on Reddy's higher-order shear deformation theory. Compos Struct 156:276–290
17. Zhang LW, Cui WC, Liew KM (2015) Vibration analysis of functionally graded carbon nanotube reinforced composite thick plates with elastically restrained edges. Int J Mech Sci 103:9–21
18. Zhang LW, Selim BA (2017) Vibration analysis of CNT-reinforced thick laminated composite plates based on Reddy's higher-order shear deformation theory. Compos Struct 160:689–705
19. Kiani Y (2016) Free vibration of FG-CNT reinforced composite skew plates. Aerosp Sci Technol 58:178–188
20. Kiani Y (2016) Free vibration of functionally graded carbon nanotube reinforced composite plates integrated with piezoelectric layers. Comput Math Appl 72:2433–2449
21. Memar Ardestani M, Zhang LW, Liew KM (2017) Isogeometric analysis of the effect of CNT orientation on the static and vibration behaviors of CNT-reinforced skew composite plates. Comput Methods Appl Mech Eng 317:341–379
22. Nejati M, Asanjarani A, Dimitri R, Tornabene F (2017) Static and free vibration analysis of functionally graded conical shells reinforced by carbon nanotubes. Int J Mech Sci 130:383–398
23. Fantuzzi N, Tornabene F, Bacciocchi M, Dimitri R (2017) Free vibration analysis of arbitrarily shaped functionally graded carbon nanotube-reinforced plates. Compos B Eng 115:384–408
24. Wang Q, Qin B, Shi D, Liang Q (2017) A semi-analytical method for vibration analysis of functionally graded carbon nanotube reinforced composite doubly-curved panels and shells of revolution. Compos Struct 174:87–109
25. Wang Q, Cui X, Qin B, Liang Q (2017) Vibration analysis of the functionally graded carbon nanotube reinforced composite shallow shells with arbitrary boundary conditions. Compos Struct 182:364–379
26. Ansari R, Torabi J, Shakouri AH (2017) Vibration analysis of functionally graded carbon nanotube-reinforced composite elliptical plates using a numerical strategy. Aerosp Sci Technol 60:152–161
27. Wang M, Li ZM, Qiao P (2018) Vibration analysis of sandwich plates with carbon nanotube-reinforced composite face-sheets. Compos Struct 200:799–809
28. Zhong R, Wang Q, Tang J, Shuai C, Qin B (2018) Vibration analysis of functionally graded carbon nanotube reinforced composites (FG-CNTRC) circular, annular and sector plates. Compos Struct 194:49–67
29. Ansari M, Kumar A, Fic S, Barnat-Hunek D (2018) Flexural and free vibration analysis of CNT-reinforced functionally graded plate. Materials 11:2387
30. Ansari R, Torabi J, Hassani R (2019) A comprehensive study on the free vibration of arbitrary shaped thick functionally graded CNT-reinforced composite plates. Eng Struct 181:653–669
31. Ghorbanpour Arani A, Kiani F, Afshari H (2019) Free and forced vibration analysis of laminated functionally graded CNT-reinforced composite cylindrical panels. J Sandw Struct Mater. https://doi.org/10.1177/1099636219830787
32. Ghorbanpour Arani A, Kiani F, Afshari H (2019) Aeroelastic Analysis of laminated FG-CNTRC cylindrical panels under yawed supersonic flow. Int J Appl Mech 11:1950052
33. Zhao J, Choe K, Shuai C, Wang A, Wang Q (2019) Free vibration analysis of functionally graded carbon nanotube reinforced composite truncated conical panels with general boundary conditions. Compos B Eng 160:225–240
34. Nguyen TN, Thai CH, Luu AT, Nguyen-Xuan H, Lee J (2019) NURBS-based postbuckling analysis of functionally graded carbon nanotube-reinforced composite shells. Comput Methods Appl Mech Eng 347:983–1003
35. Mohammadimehr M, Monajemi A, Afshari H (2017) Free and forced vibration analysis of viscoelastic damped FG-CNT reinforced micro composite beams. Microsyst Technol 23:1–15
36. Shen HS (2009) Nonlinear bending of functionally graded carbon nanotube-reinforced composite plates in thermal environments. Compos Struct 91(1):9–19
37. Mindlin RD (1951) Influence of rotary inertia and shear on flexural motion of isotropic elastic 37 plates'. J Appl Mech Trans Asme 18:31–38
38. Zare Jouneghani F, Dimitri R, Bacciocchi M, Tornabene F (2017) Free vibration analysis of functionally graded porous doubly-curved shells based on the first-order shear deformation theory. Appl Sci 7:1252
39. Reddy JN (2004) Mechanics of laminated composite plates and shells: theory and analysis. CRC Press, Boca Raton
40. Reddy JN (2017) Energy principles and variational methods in applied mechanics. Wiley, Hoboken
41. Bellman R, Casti J (1971) Differential quadrature and long-term integration. J Math Anal Appl 34:235–238
42. Tornabene F, Fantuzzi N, Ubertini F, Viola E (2015) Strong formulation finite element method based on differential quadrature: a survey. Appl Mech Rev 67:020801
43. Karami B, Janghorban M, Dimitri R, Tornabene F (2019) Free vibration analysis of triclinic nanobeams based on the differential quadrature method. Appl Sci 9:3517
44. Torabi K, Afshari H, Aboutalebi FH (2014) A DQEM for transverse vibration analysis of multiple cracked non-uniform Timoshenko beams with general boundary conditions. Comput Math Appl 67:527–541
45. Afshari H, Rahaghi MI (2018) Whirling analysis of multi-span multi-stepped rotating shafts. J Braz Soc Mech Sci Eng 40:424
46. Bert CW, Malik M (1996) Differential quadrature method in computational mechanics: a review. Appl Mech Rev 49:1
47. Du H, Lim MK, Lin RM (1994) Application of generalized differential quadrature method to structural problems. Int J Numer Meth Eng 37:1881–1896

48. Liew KM, Xiang Y, Kitipornchai S, Wang C (1998) Vibration of Mindlin plates: programming the p-version Ritz method. Elsevier, Amsterdam
49. Romero G, Alvarez L, Alanís E, Nallim L, Grossi R (2003) Study of a vibrating plate: comparison between experimental (ESPI) and analytical results. Opt Lasers Eng 40:81–90